Building Lagrangian injectors from resolved primary atomization simulations. Application to jet in crossflow fuel injection

Carlos Guillamon, Romain Janodet, Léa Voivenel, Renaud Mercier, Vincent Moureau

Building Lagrangian injectors from resolved primary atomization simulations. Application to jet in crossflow fuel injection

Carlos GUILLAMON[1,2], Romain JANODET[1,3], Léa VOIVENEL[1],
Renaud MERCIER*[1], Vincent MOUREAU[3]
[1]Safran Tech, Rue des Jeunes Bois, Châteaufort, 78114 Magny-les-Hameaux, France
[2]CERFACS, 42 Avenue Gaspard Coriolis, 31057 Toulouse, France
[3]CORIA, CNRS UMR6614, INSA and University of Rouen, Avenue de l'Université,
76801 Saint-Etienne-du-Rouvray, France
*Corresponding author email: renaud-c.mercier@safrangroup.com

Abstract
This work aims at improving Lagrangian particle injectors for the simulation of sprays. In such simulations, primary atomization is not resolved and Lagrangian particles are directly injected as a dispersed phase in the flow. Two main challenges arise in such methodology: i) the prescription of the correct droplet size and velocity distributions at injection, ii) ensuring the proper coupling of the dispersed phase with the gas phase to have the correct gas flow field after the injection. The proposed approach relies on an improved Lagrangian injector model and on resolved primary atomization simulations to feed the injector model parameters. The resolved atomization simulations are performed using a sharp-interface approach (ACLS/GFM) on unstructured grids [1, 2]. The validation test case is a high-pressure, non-reactive kerosene jet in crossflow (JICF) atomizer configuration [3], which is representative of complex injection systems. Resolved simulations of atomization for this configuration are performed and validated against the experimental correlation for the jet trajectory, showing good accordance. These simulations are then post-processed to feed the Lagrangian injector model. Finally, the injectors are applied to the same configuration and compared to experimental data.

Keywords
Atomization, level set, Lagrangian injection, dispersed multiphase flows, jet in crossflow.

Introduction
Simulations of aeronautical combustion chambers require an accurate description of the liquid fuel dispersion which has a strong influence on the flame. However, computations comprising all the physical processes from injection to combustion cannot be achieved within the same simulation due to the wide range of scales. Approaches aiming at resolving primary atomization, such as diffuse or sharp interface methods [1, 2], can accurately resolve the liquid-gas interface. However, they become very expensive when many small droplets are present and when these have to be transported over long distances. Other formalisms, such as Lagrangian point-particle methods [4], can be applied to reactive computations at the expense of considering an already atomized spray. Consequently, they require a proper modeling of atomized spray injection, whose modeling parameters often comes from experimental measurements not always available in practical situations.
In order to improve the modeling of fuel injection in complex aeronautical systems, a new methodology to build injectors for dispersed phase computations has been developed. The aim of these injectors is to correctly reproduce the droplet size and velocity distributions in time and space but also the impact of the liquid jet presence and its atomization on the gas flow, which may then influence the spray dispersion. This latter is difficult as it requires to model the momentum exchanges between the carrier phase and the injected liquid fuel that undergoes atomization. To get the correct space/time droplet size/velocity distribution of the largest droplets and the momentum exchanges between the gas and the liquid, resolved atomization simulations are performed and post-processed. Eventually, the proposed Lagrangian injector

model learns the spray characteristics just after primary atomization from the resolved atomization simulations and can then be used to inject accurately Lagrangian droplets in combustion simulations. The strategy is first developed on a non-reactive liquid jet in air crossflow tested experimentally by Becker and Hassa [3]. The blockage effect from the liquid dense core to the gas, which creates vortical structures affecting droplet dispersion [5], is characterized in the resolved simulations and modeled with the Actuator Line Method (ALM) [6]. The secondary atomization model by Gorokhovski [7] is embedded in the dispersed phase simulations. The models are then applied to the configuration and compared with existing experimental data.

Building Lagrangian injectors from resolved atomization simulations

This section describes the proposed strategy to build Lagrangian injectors for dispersed phase simulations. First, **resolved atomization simulations** are performed with an Accurate Conservative Level-Set (ACLS) methodology [1] on unstructured grids [2] (Fig. 1 left). The resulting spray is retrieved and processed as follows:

1. Particles are tracked by their centroid, sampled when they cross a specific slice in space perpendicular to the crossflow (sampling plane), and accumulated with time (Fig. 2 left). Collected statistics are droplet volume $\mathrm{V_{dr}}$, centroid position $\mathbf{x}_{\mathrm{dr}}$ and velocity $\mathbf{u}_{\mathrm{dr}}$. An equivalent diameter $\mathrm{d_{dr}}$ is defined from the volume: $\mathrm{d_{dr}} = \sqrt[3]{6\mathrm{V_{dr}}/\pi}$.

2. Statistical convergence of the spray is verified to ensure that enough droplets have been accumulated. The droplet size histogram f_n, where n denotes the n_{th} size class, is obtained at several accumulation times t_i and compared quantitatively to the spray at the last accumulation time t_{acc} with a Mean Squared Error (MSE) criterion [8]: $\mathrm{MSE}^{t_i} = 1/\mathrm{N}\sum_{n=1}^{\mathrm{N}}\left(f_n^{t_i} - f_n^{t_{\mathrm{acc}}}\right)^2$, where N is the number of classes in the histogram. Convergence is achieved when the MSE normalized by its maximum does not change significantly as more droplets are accumulated: $\mathrm{MSE}^{t_i}/\max_{t_i}(\mathrm{MSE}) < \varepsilon$, where ε has been set to 0.03.

3. Droplets are classified spatially on rectangular probes to get an in-plane repartition of size/velocity distributions (Fig. 2 right). Each probe (j,k) contains an individual spray characterized by its own size histogram $f_{j,k}$ and Sauter Mean Diameter $\mathrm{SMD}_{j,k}$, mean and root-mean squared (RMS) velocities $\overline{\mathbf{u}}_{j,k}$, $\mathbf{u}_{\mathrm{RMS,j,k}}$, and liquid flux.

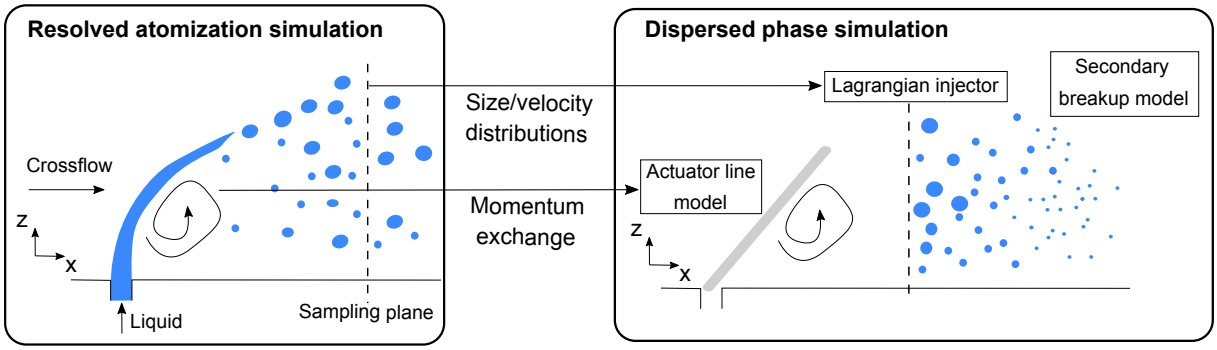

Figure 1. Flowchart of the proposed methodology.

Once the atomized spray has been processed, a Lagrangian injector is defined for the **dispersed phase simulations** (Fig. 1 right). This injector can prescribe the droplets injection location $\mathbf{x}_{\mathrm{inj}}$ (randomly distributed within each probe), sizes $\mathrm{d_{inj}}$ (varying diameter by sampling from $f_{j,k}$, or constant size given by $\mathrm{SMD}_{j,k}$), velocities $\mathbf{u}_{\mathrm{inj}}$ (constant mean values, or a combination of both mean and RMS) and fluxes (Fig. 2 right). Droplets are assumed to be rigid and spherical, and their dynamics are governed by the point-particles equations of motion [4] with two-way coupling through the drag force.

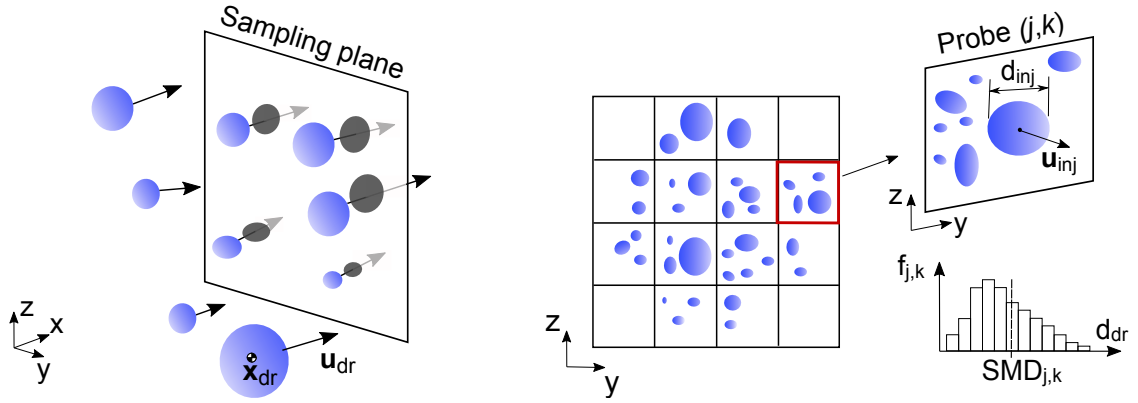

Figure 2. *Left*: droplet sampling in planes perpendicular to the crossflow from resolved atomization simulations. Accumulated droplets are projected as grey circles. *Right*: classification of droplets in probes to get size/velocity distributions in space.

Additionally, the momentum exchange between the jet coherent structures (dense core) and the gaseous phase is modeled. The dense core creates a strong blockage effect which is present in the resolved atomization simulation, but not in the dispersed phase one. This effect is firstly estimated from the former by calculating the net force exerted to the dense core as $|\mathbf{F}_{\text{core}}| = (p_{\text{windward}} - p_{\text{leeward}})\,\text{S}_{\text{core}}$, where S_{core} is the dense core cross-section, and p_{windward} and p_{leeward} are the mean gas pressures at the windward and leeward sides respectively (Fig. 3 left). This force has an inclination θ due to the bending of the liquid column by action of the air. Then, the Actuator Line Method (ALM) [6] is applied to impose body forces in the dispersed phase simulation. These forces are located at discrete points distributed along a line of length L and inclination θ (same value as the inclination of $\mathbf{F}_{\text{core}}$), called actuator, which mimics the location of the dense core. The actuator is discretized into elements of width w, and the force application points p are located at each element center x_p,z_p (Fig. 3 right). A body force $\mathbf{F}(x_p,z_p)$ with same direction as $\mathbf{F}_{\text{core}}$ is imposed to each point. This force increases linearly along the actuator to account for the actual increase in cross-sectional area of the dense core [9]. The sum of all body forces equals the dense core net force: $\sum_p \mathbf{F}(x_p,z_p) = \mathbf{F}_{\text{core}}$.
Finally, a secondary breakup model is embedded in the dispersed phase simulations to consider further atomization of Lagrangian droplets when they are not in equilibrium with the ambient gas [10]. In this work, the stochastic breakup model of Gorokhovski is used [7].

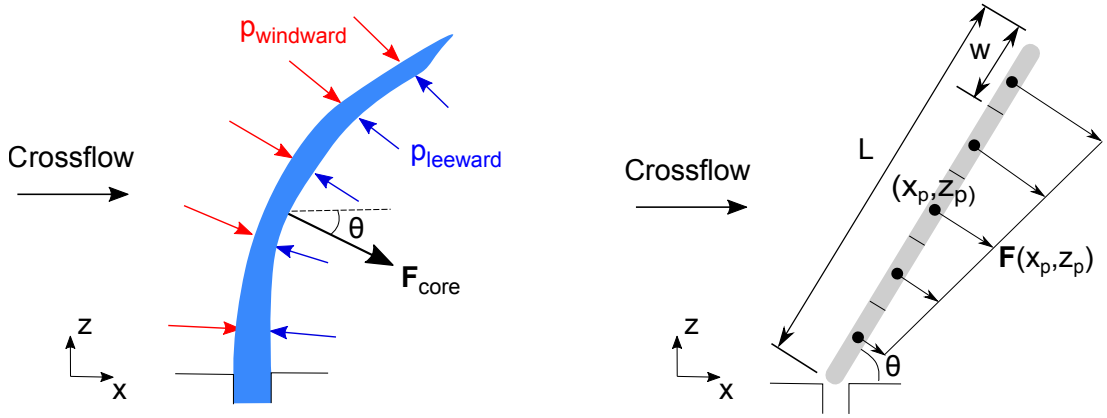

Figure 3. *Left*: schematic resolved dense core, showing the pressure distribution in the windward (red arrows) and leeward (blue arrows) sides, and the net force F_{core}. *Right*: actuator line model representing the dense core in dispersed phase simulations.

Numerical methods for resolving atomization

ACLS/GFM framework for interface capturing on adaptive unstructured grids

Primary atomization is numerically solved with the Accurate Conservative Level-Set (ACLS) interface-capturing technique [1, 11]. The extension of the up-to-date method to adaptive unstructured grids has been performed in [2]. The ACLS methodology distinguishes liquid and gaseous phases by defining a hyperbolic-tangent function $\psi(\mathbf{x},t) = 1/2\left(\tanh\left(\phi(\mathbf{x},t)/2\varepsilon\right)+1\right)$, where the parameter ε sets the thickness of the profile, and $\phi(\mathbf{x},t) = \pm|\mathbf{x}(t)-\mathbf{x}_\Gamma(t)|$ is the signed-distance function. The liquid-gas interface Γ is located at the iso-value $\psi = 1/2$, see Fig. 4 left. This function ψ is transported by the fluid:

$$\frac{\partial \psi}{\partial t} + \nabla\cdot\left(\psi\mathbf{u}\right) = 0 \tag{1}$$

where the velocity field $\mathbf{u}$ is divergence free: $\nabla\cdot\mathbf{u} = 0$. After transport, the reinitialization equation of [11] is applied:

$$\frac{\partial \psi}{\partial \tau} = \nabla\cdot\left(\frac{1}{4\cosh^2\left(\phi_{\text{map}}/2\varepsilon\right)}\left(|\nabla\phi_{\text{map}}\cdot\mathbf{n}|-1\right)\mathbf{n}\right) \tag{2}$$

where $\phi_{\text{map}} = \varepsilon\ln\left(\psi/(1-\psi)\right)$ is an analytical signed-distance function mapped for $\psi\in]0;1[$, τ is a pseudo-time, and $\mathbf{n}$ is the normal vector field to the interface. This reinitalization equation ensures that the hyperbolic tangent profile ψ is reshaped after transport without introducing significant spurious displacement of the interface. The ACLS methodology is coupled to the Ghost-Fluid Method (GFM) [12] in order to deal explicitly with the pressure jump at the interface:

$$\left[p\right]_\Gamma = p_{l,\Gamma} - p_{g,\Gamma} = \sigma\kappa_\Gamma + 2\left[\mu\right]_\Gamma \mathbf{n}^{\mathrm{T}}\cdot\nabla\mathbf{u}\cdot\mathbf{n} \tag{3}$$

where κ_Γ is the interface mean curvature and μ is the dynamic viscosity. Using this formulation, surface tension forces $\sigma\kappa_\Gamma$ are embedded in the pressure jump.

Dynamic mesh adaptation

To better resolve the atomization dynamics and save computational resources, the ACLS/GFM method is coupled to an Adaptive Mesh Refinement (AMR) strategy for increasing the mesh resolution at the liquid-gas interface at an affordable cost. In AMR, the target element size at the interface Δx_{min} and N_p, the number of cells with this minimum size in the half-width of the refined region, are user-defined parameters, see Fig. 4 right. The mesh is dynamically refined throughout the computation with an automatic distance-based triggering ensuring that the interface always remains within the region of element size Δx_{min} [13]. In the vicinity of this region, the cell size increases linearly with controlled slope until the coarser cell size Δx_{init}.

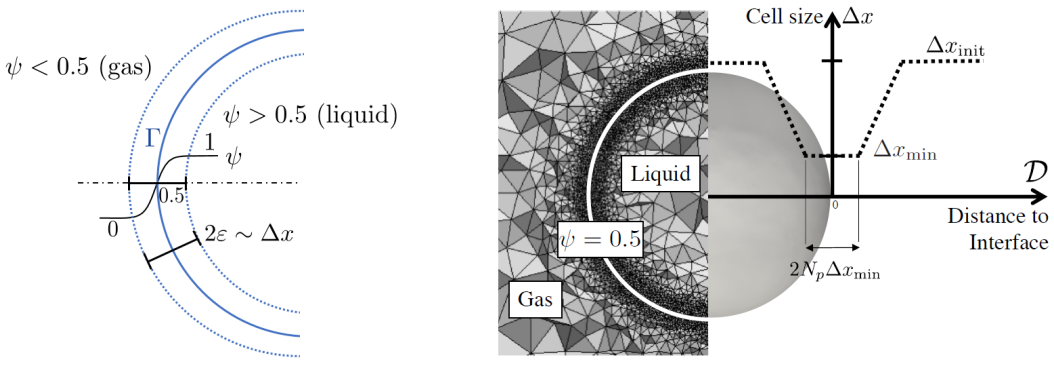

Figure 4. *Left*: interface representation in ACLS [14]. *Right*: Illustration of dynamic mesh adaptation with AMR [13]

Test case and computational setup

The experimental test case chosen to simulate fuel injection is a high-pressure kerosene jet in air crossflow tested by Becker and Hassa [3]. It is selected for its application in multipoint injectors for aeronautical combustion chambers. The numerical domain replicating the test bench is shown in Fig. 5. It consists of a plenum where pressurized air (the crossflow) is introduced through a gaseous inlet. Kerosene is injected perpendicularly to the crossflow through a tapered nozzle located at the bottom of the plenum. A Poiseuille velocity profile is prescribed at the liquid inlet. For crossflow injection, it was experimentally observed that the boundary layer thickness at the lip of the injector is 5 mm [3]. As the numerical domain is reduced with respect to the experimental bench, a velocity profile with a boundary layer following a 1/7th power law is prescribed. The thickness of this boundary layer is calculated considering that the gas evolves from the inlet to the injector as a turbulent boundary layer along a flat plate. Outside the boundary layer, the velocity follows a parabolic profile. The operating point of the jet in crossflow is governed by two dimensionless numbers: the momentum ratio $\mathrm{q} = \rho_l u_l^2/(\rho_g u_g^2)$ and the gaseous Weber number $\mathrm{We}_g = \rho_g u_g^2 d_{\mathrm{inj}}/\sigma$. The operating condition is the baseline case reported in [3]: $\mathrm{q} = 6$ and $\mathrm{We}_g = 1470$, making $u_l = 23.33$ m/s and $u_g = 100$ m/s. According to these values, both column and surface breakup mechanisms of atomization are present [15]. Two simulations are performed with interface resolutions Δx_{min} of 20 μm (coarse case) and 10 μm (fine case).

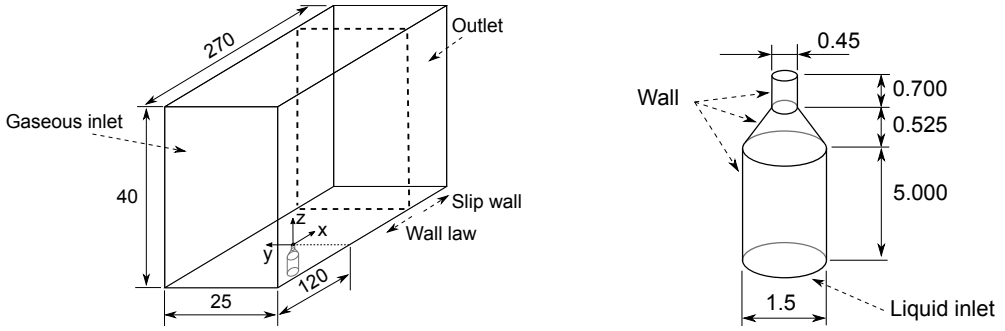

Figure 5. Setup and boundary conditions replicating the experimental facility tested in [3]. *Left*: complete domain. *Right*: detailed view of the injection nozzle

Results and discussion

Resolved simulations of jet in crossflow atomization

Jet in crossflow simulations performed with the ACLS/GFM methodology are validated with the experimental correlation for the trajectory of the jet's windward side provided by [3]:

$$\frac{z}{d_{\mathrm{inj}}} = 1.57\mathrm{q}^{0.36}\ln\left(1 + 3.81\frac{x}{d_{\mathrm{inj}}}\right) \tag{4}$$

which depends on q and d_{inj}. Results are shown in Fig. 6 left. Both resolutions show a good agreement with experiments close to the injector, despite a slight underestimation for the coarse case Δx_{min} = 20 μm. This tendency is maintained up to a given location downstream the injection point, from where both simulations overestimate the experimental results. The coarse and fine simulations surpass the experimental trajectory at x ~ 6 mm and x ~ 3 mm, respectively: for all axial locations, the former case penetrates lower than the later. This difference in penetration between resolutions is attributed to liquid separation from the walls inside the nozzle, which has been observed at the exit of the nozzle's convergent section for the fine resolution. Liquid detachment contracts the jet, hence reducing its effective area and increasing the velocity due to mass conservation. This phenomenon is captured in the fine case but not in the coarse one because the boundary layer within the injector is better resolved in the former than in the latter. The occurrence of this internal flow effect is attributed to nozzle geometry features such as the nozzle's low L/D ratio or the contraction from the liquid inlet cross-section to the injection area at the plenum [16], see Fig. 5 right.

Instantaneous snapshots of the established jets for both resolutions are shown in Fig. 6. A good qualitative behavior is observed. Liquid injected bends towards the gas streamwise direction due to momentum exchange with the crossflow. Instabilities leading to primary atomization are observed in the windward side of the main liquid column (the dense core), which lead to the rupture of the jet into big ligaments: this is the column breakup mechanism. Simultaneously, small droplets are stripped-off along the liquid dense core due to strong shear force caused by the air: this atomization mechanism is known as surface breakup. Ligaments generated by column breakup will continue breaking into smaller structures and droplets as they are convected downstream, whereas droplets generated by surface breakup are small and will not further atomize [17]. The lower penetration of the case $\Delta x_{\min}$ = 20 µm is observed, as well as the difference in size of the resolved liquid structures: the case $\Delta x_{\min}$ = 10 µm shows a larger number of droplets due to its finer resolution.

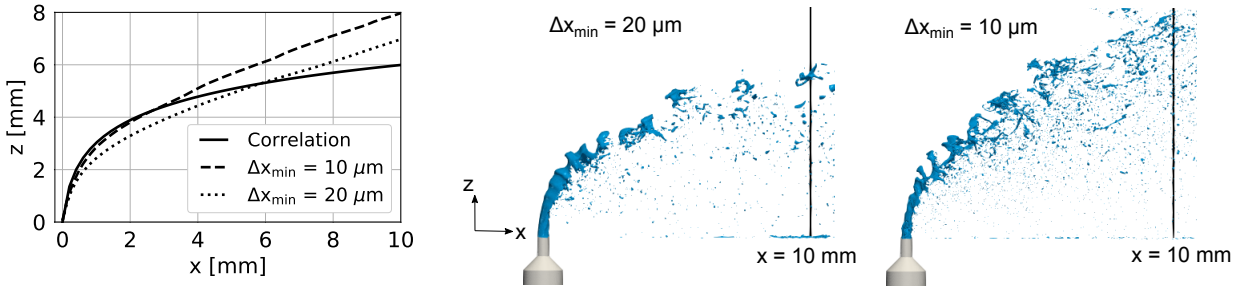

Figure 6. *Left*: mean trajectories of the computed jet compared to the experimental correlation by [3]. *Center and right*: instantaneous snapshots of jet simulation with $\Delta x_{\min}$ = 20 µm and 10 µm, respectively.

Building Lagrangian injectors

Spray from the JICF resolved atomization simulations is sampled in planes perpendicular to the crossflow. Fig. 6 shows a sampling plane at x = 10 mm downstream the injection nozzle for both resolutions. For building injectors, the spray sampled from the fine resolution $\Delta x_{\min}$ = 10 µm is used. The location x = 10 mm is chosen since a finely atomized spray is found here, while primary atomization is taking place further upstream with the presence of ligaments and blobs. Furthermore, this location is the first plane downstream where a converged spray according to the MSE criterion is obtained. A total of 9,100 droplets has been accumulated at this location. Then, droplets are classified spatially to produce an in-plane characterization of the spray, shown in Fig. 7. Three parameters are displayed: Sauter Mean Diameter (SMD), fuel volume flux and mean axial velocity (in crossflow direction). The SMD map (Fig. 7 left) shows that droplets size increases along the vertical direction. Small SMD values at the bottom correspond to droplets generated by surface breakup, while the largest ligaments emanating from the dense core due to column breakup are located in the upper region. A decrease in SMD in the top part of the spray is observed, which is attributed to small droplets being from the column ligaments, see Fig. 6 right. The liquid volume flux (Fig. 7) exhibits a circular pattern as expected from the experiments. Regarding the mean axial velocity (Fig. 7 right), low velocities are found at the central, bottom part of the spray plume. This is the area affected by the wake generated by the dense core (blockage effect), causing droplet's deceleration. High velocities are seen at the edges of the bottom part, which are attributed to acceleration by the crossflow of the small droplets generated by surface breakup, since they have a lower relaxation time than big droplets located at the top part. These spray structures in planes perpendicular to the crossflow have been observed in experimental studies [3, 15].

The spatially distributed statistics shown in Fig. 7 define the Lagrangian injectors to initialize dispersed phase simulations. Besides the displayed parameters, RMS liquid axial velocities, and both mean and RMS lateral and vertical velocities, can be calculated and represented in the same way (not shown here).

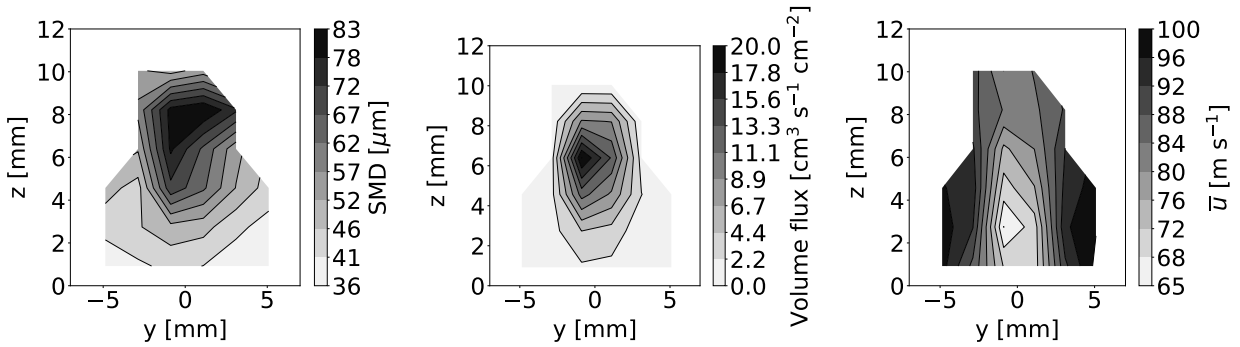

Figure 7. Spatially distributed spray statistics at x = 10 mm. *Left*: Sauter Mean Diameter (SMD). *Center*: liquid volume flux. *Right*: liquid mean axial velocity in crossflow direction

Application to a dispersed phase simulation

A dispersed phase simulation has been performed by injecting the spray distributions at x = 10 mm. Sizes and fluxes are respectively given by the left and center maps of Fig. 7. Velocities are specified as a combination of both mean and RMS velocities in each direction: $\mathbf{u}_{\text{inj}} = \overline{\mathbf{u}} + \mathbf{r}^{\text{T}}\mathbf{u}_{\text{RMS}}$, where $\mathbf{r}$ is a vector of random numbers following a normal distribution with mean 0 and standard deviation 1. The dense core blockage effect is taken into account with an actuator where discretely distributed body forces are applied. Two-way coupling for momentum exchange between phases is considered.

The simulation is validated against the experiments by comparing the fuel volume flux maps at x = 80 mm, see Fig. 8. As in the experimental case, both symmetry with respect to the y axis and a circular flux pattern are observed. Lateral and vertical spray bounds are similar in both cases. However, the spray penetration is overestimated in the simulation: the obtained volume flux distribution and the vertical location of maximum flux are shifted upwards. The numerical spray is more dispersed in the plane, hence reducing the values of maximum flux with respect to the experiments. These differences are due to the penetration overestimation in the simulation with respect to the experiments, as shown in Fig. 6.

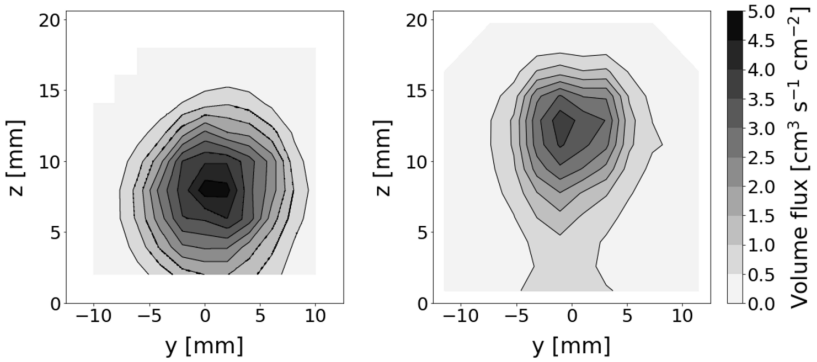

Figure 8. Volume flux maps at x = 80 mm downstream the injection nozzle. *Left*: experimental map from [3]. *Right*: dispersed phase simulation map.

Conclusions

This work shows a new methodology to develop models for injection of Lagrangian droplets. Its main advantages with respect to other Lagrangian injection models [18, 19] are its capability to perform full two-phase Lagrangian simulations without the need to resolve atomization once the spray state is known, allowing in the future to initialize reactive cases with evaporation and combustion; to use one numerical code for resolving atomization and another one for dispersed phase (e.g. combustion) simulations; and to model the aerodynamic field in dispersed phase simulations caused by coherent liquid structures without the need of resolving atomization. The spray from resolved atomization simulations is processed to obtain size/velocity distributions in

space that are injected in dispersed phase computations. The models are complemented with inclusion of the dense core blockage effect and an embedded secondary breakup model in the dispersed phase simulations. The full methodology is applied to a liquid jet in crossflow tested experimentally in [3]. Two resolved atomization simulations of this configuration have been performed for two different interface cell sizes, giving good results qualitatively on jet topology and breakup and quantitatively on mean jet penetration close to the injection location. Finally, injectors are created and applied to a dispersed phase computation. Comparison with experiments show that the circular shape of volume flux is retrieved, but that the actual spray pattern and maximum flux values are not well captured. Choosing a different injection location, improvements in the modeling of the dense core blockage effect or inclusion of turbulent dispersion models could help to improve these results. It is also believed that the gaseous inlet velocity profile can influence the resolved simulations, as well as the addition of synthetic turbulence. Future work includes investigating these effects and the application of the developed models to other operating conditions [3].

Acknowledgements

This project has received funding from the European Union Horizon 2020 research and innovation program under the Marie Sklodowska-Curie grant agreement No. 765998 in the project ANNULIGhT. Computer resources have been provided by GENCI, France, under the allocation A0092B11072. The authors also gratefully acknowledge Pr. Thierry Poinsot from CERFACS, France, for fruitful discussions on the models presented in this article.

References

[1] Desjardins, O., Moureau, V., Pitsch, H., 2008, *J. Comput. Phys.*, 227, pp. 8395-8416.
[2] Janodet, R., Guillamon, C., Moureau, V., Mercier, R., Lartigue, G., Benard, P., Menard, T., Berlemont, A., 2020, ⟨*hal-03024186*⟩.
[3] Becker, J., Hassa, C., 2002, *Atomization and Sprays*, 11, pp. 49-67.
[4] Maxey, M., Riley, J. 1983, *Physics of Fluids*, 26 (4), pp. 883-889.
[5] Arienti, M., Madabhushi, R. K., Van Slooten, P. R., Soteriou, M. C., May 8.-11., ASME Turbo Expo 2006: Power for Land, Sea and Air.
[6] Sørensen, J. N., Shen, W. Z., 2002, *Journal of Fluid Engineering*, 124, pp. 393-399.
[7] Gorokhovski, M., 2001, *Atomization and Sprays*, 11, pp. 505-519.
[8] Anderson, T. W., 1962, *Annals of Mathematical Statistics*, 33 (3), pp. 1148-1159.
[9] Mashayek, A., Jafari, A., Ashgriz, N., May 23.-26. 2006, 19th Annual Conference on Liquid on Liquid Atomization and Spray Systems.
[10] Lefebvre, A. H., McDonell, V. G., 2017, "Atomization and Sprays". CRC Press.
[11] Chiodi, R., Desjardins, O., 2017, *J. Comput. Phys.*, 343, pp. 186-200.
[12] Fedkiw, R., Aslam, T., Merriman, B., Osher, S., 1999, *J. Comput. Phys.*, 152(2), pp. 457-492.
[13] Leparoux, J., Mercier, R., Moureau, V., Musaefendic, H., July 22.-26. 2018, 14th Triennal International Conference on Liquid Atomization and Spray Systems
[14] Janodet, R., Vaudor, G., Lartigue, G., Bénard, P., Moureau, V., Mercier, R., Sep. 2.-4. 2019, 29th European Conference on Liquid Atomization and Spray Systems.
[15] Wu, P.-K., Kirkendall, K. A., Fuller, R. P., Nejad, A. S., 1997, *J. Prop. Power*, 13 (1), pp. 64-73.
[16] Reitz, R. D., Bracco, F. V., 1982, *Physics of Fluids*, 25, pp. 1730-1742.
[17] Rachner, M., Becker, J., Hassa, H., Doerr, T., 2002, *Aerospace Science and Technology*, 6, pp. 495-506.
[18] Herrmann, M., 2010, *J. Comput. Phys.*, 229, pp. 745-759.
[19] Fontes, D.H., Vilela, V., Meira, L. S., Souza, F. J., 2019, *Int. J. Mul. Flow*, 114, pp. 98-114.